

# A Global-Local Optimization Framework for Simultaneous Multi-Mode Multi-Corner Clock Skew Variation Reduction

Kwangsoo Han<sup>‡</sup>, Andrew B. Kahng<sup>†‡</sup>, Jongpil Lee<sup>\*</sup>, Jiajia Li<sup>‡</sup> and Siddhartha Nath<sup>†</sup>

<sup>†</sup>CSE and <sup>‡</sup>ECE Departments, UC San Diego, <sup>\*</sup>Samsung Electronics Co. Ltd.  
{kwhan, abk, jil150, sinath}@ucsd.edu, jongpil0.lee@samsung.com

## ABSTRACT

As combinations of signoff corners grow in modern SoCs, minimization of clock skew variation across corners is important. Large skew variation can cause difficulties in multi-corner timing closure because fixing violations at one corner can lead to violations at other corners. Such “ping-pong” effects lead to significant power and area overheads and time to signoff. We propose a novel framework encompassing both global and local clock network optimizations to minimize the sum of skew variations across different PVT corners between all sequentially adjacent sink pairs. The global optimization uses linear programming to guide buffer insertion, buffer removal and routing detours. The local optimization is based on machine learning-based predictors of latency change; these are used for iterative optimization with tree surgery, buffer sizing and buffer displacement operators. Our optimization achieves up to 22% total skew variation reduction across multiple testcases implemented in foundry 28nm technology, as compared to a best-practices CTS solution using a leading commercial tool.

## Categories and Subject Descriptors

B.7.2 [Hardware]: INTEGRATED CIRCUITS—*Design Aids*

## General Terms

Algorithms, Design, Optimization

## 1. INTRODUCTION

Modern SoCs typically exploit complex operating scenarios to maximize performance and reduce power consumption. For instance, techniques such as dynamic voltage and frequency scaling (DVFS), split rail power supply, etc. are widely applied in SoC designs to meet performance and power targets. However, these techniques increase the number of modes and corners used for timing closure, which will in turn lead to increased datapath delay variation and clock skew variation across corners. Such large timing variations increase area and power overheads, as well as design turnaround time (TAT) due to a “ping-pong” effect whereby fixing timing issues at one corner leads to violations at other corners. To solve this issue, we can minimize either datapath delay variation or *clock skew variation* across corners. Given that datapath optimization is a local optimization and is usually applied after the clock network optimization, what datapath delay variation minimization can accomplish is limited. In other words, datapath optimizations are practically less impactful than minimizing clock skew variations in most cases. This is why clock network optimization is a key first step during the physical implementation flow for timing closure. Further, clock skew variation can be achieved via both global and local optimizations of the clock network. Therefore, minimizing clock skew variation across corners is more effective for multi-corner timing closure. In this work, we minimize clock skew variation.

Moreover, timing violations due to clock skew variation across corners are typically reduced by (hold and/or setup) buffer insertion,  $V_{th}$ -swapping and gate sizing on datapaths at later

design stages. Thus, clock skew variation between each pair of sequentially adjacent sinks can lead to potential costs of area, power and design TAT. We therefore minimize the sum of skew variations between all sink pairs to minimize the overall physical implementation costs (e.g., in area, power, TAT).

Although many commercial EDA tools are capable of multi-mode multi-corner clock network synthesis [21] [25], our optimization framework can be applied as an incremental optimization for further reduction of skew variations in light of our robust interface to commercial P&R and STA tools. Moreover, experimental results show that our proposed optimization is able to achieve significant skew variation reduction on clock networks that have been synthesized with a leading commercial tool.

Contributions of our work are as follows.

1. We are the first in the literature to study the problem of minimizing the *sum of clock skew variations* across multiple PVT corners.
2. We propose a novel global-local framework for clock network optimizations to minimize the sum, over all pairs of PVT corners, of skew variation between all sequentially adjacent pairs.
3. We demonstrate that machine learning-based predictors of latency change can provide accurate guidance on the best moves to test during local optimization for minimization of skew variation across corners.
4. Our optimization framework has a robust interface to leading commercial P&R and STA tools and production PDKs/libraries, and can be generalized to other clock network optimization problems.
5. We achieve up to 22% reduction in the sum of skew variations of clock trees in testcases that reflect high-speed application processor and memory controller blocks.

## 2. RELATED WORK

We classify previous works on clock skew optimization as (i) works that target skew and/or delay optimization at single or multiple corners, and (ii) works that optimize skew variation across multiple PVT corners.

Several previous works optimize skew at one or more PVT corners, but do not address skew variation across corners. Cao et al. [4] minimize the worst skew in a clock tree by partitioning the tree into different skew groups. The authors then greedily minimize the worst skew in each skew group to minimize overall local skew. Cho et al. [6] perform clock tree optimization that is temperature-aware. The authors modify the deferred merge embedding (DME) algorithm to include *merging diamonds* for consideration of temperature variations to guide clock skew and wirelength minimization. Lung et al. [10] perform multi-mode multi-corner (MMMC) clock skew optimization by minimizing the worst skew across all corners. They propose a methodology to determine the *delay correlation factor* for clock buffers at 130nm, 90nm and 65nm and conclude that the correlation across corners is linear. However, such an assumption might not be valid at 28nm and below. Lung et al. [11] perform chip-level as well as module-level clock skew optimizations with multiple voltage modes. The authors use power-mode-aware buffers for chip-level clock tree optimization. For the module-level optimization, they only consider the worst voltage corner.

Relatively fewer works exist that optimize skew variation across multiple PVT corners. Restle et al. [18] propose a two-dimensional nontree structure. They divide the nontree structure into two levels – leaf level (close to clock sinks) and top level (close to clock source). The top level is the same as the traditional clock tree

Permission to make digital or hard copies of all or part of this work for personal or classroom use is granted without fee provided that copies are not made or distributed for profit or commercial advantage and that copies bear this notice and the full citation on the first page. Copyrights for components of this work owned by others than ACM must be honored. Abstracting with credit is permitted. To copy otherwise, or republish, to post on servers or to redistribute to lists, requires prior specific permission and/or a fee. Request permissions from Permissions@acm.org.  
DAC'15, June 07 - 11 2015, San Francisco, CA, USA.  
Copyright 2015 ACM 978-1-4503-3520-1/15/06 ...\$15.00.  
<http://dx.doi.org/10.1145/2744769.2744776>.

structure, but the leaf level is a mesh structure such that each sink is connected to the nearest point on the mesh. Although this is a very effective way to minimize skew variation across corners, the mesh structure consumes enormous wire resources and power. Su and Sapatnekar [20] use mesh structures for the top-level tree which consumes less wire resource and power as compared to [18]. However, this consumes 59%-168% more wire resource than a tree structure. Further, the authors do not optimize skew variation which still exists in the bottom-level subtrees. Rajaram et al. [16] [17] propose a nontree construction method to insert crosslinks<sup>1</sup> in a clock tree by estimating subtree delays using the Elmore delay model. The authors verify their method with SPICE-based Monte Carlo simulations and report skew variability reduction. However, the approach consumes excess additional wire and power due to crosslink insertions. Mittal and Koh [15] propose a greedy method to insert crosslinks to reduce skew variation.

To our knowledge, there has been no systematic framework for minimization of *clock skew variation* (across multiple signoff corners) for clock trees. Our work exploits both global and local iterative optimizations to minimize skew variations across different PVT corners which is very important for high-speed processor and multimedia blocks that operate at multiple modes/corners. Further, instead of minimizing the maximum skew or skew variation, we minimize the sum of skew variations over all sink pairs, which will reduce the potential costs of gate sizing and buffer insertion for multi-corner timing closure.

### 3. PROBLEM FORMULATION

The notations we use in this paper are given in Table 1.

**Table 1: Description of notations used in our work.**

Term	Meaning
$c_k$	operating corner, ( $0 \leq k \leq K$ ; $c_0$ is the nominal corner)
$\alpha_k$	normalization factor of corner $c_k$ with respect to $c_0$
$f_i$	sink (e.g., flip-flop) in clock tree, ( $1 \leq i \leq N$ )
$P_i$	clock path from clock source to $f_i$
$skew_{i,i'}^{c_k}$	clock skew between sink pair $(f_i, f_{i'})$ at corner $c_k$
$s_j$	arc (i.e., tree segment without branching) in clock tree, ( $1 \leq j \leq M$ )
$D_j^k$	original arc delay at corner $c_k$
$\Delta_j^k$	delay change of arc $s_j$ at corner $c_k$ from optimization
$D_{j,max}^k$	maximum latency of a clock path at corner $c_k$
$v_{i,i'}^{c_k,c_{k'}}$	normalized skew variation across corner pair $(c_k, c_{k'})$ between $(f_i, f_{i'})$
$V_{i,i'}$	worst normalized skew variation across all corner pairs between $(f_i, f_{i'})$

For a corner pair  $(c_k, c_{k'})$ , we define the normalized skew variation between sink pair  $(f_i, f_{i'})$  as

$$v_{i,i'}^{c_k,c_{k'}} = |\alpha_k \cdot skew_{i,i'}^{c_k} - \alpha_{k'} \cdot skew_{i,i'}^{c_{k'}}| \quad (1)$$

where skew ( $skew_{i,i'}^{c_k}$ ) is defined as the latency difference between capture and launch clock paths at  $c_k$ . We emphasize that our optimization is local skew-aware, so that we only optimize skews between launch-capture sink pairs that have valid datapaths in between them (i.e., we avoid the pessimism that would result from use of global skew in the formulation).  $\alpha_k$  is the normalization factor at corner  $c_k$  with respect to the nominal corner. Note that  $\alpha_k$  is an input parameter and can be determined by technology information (e.g., ratio between buffer delays at  $c_k$  and  $c_0$ ), clock tree properties (e.g.,  $V_{th}$  and sizes of buffers in the tree), etc. Further, one can define specific  $\alpha_k$  values for each sink pair. In our work, we define  $\alpha_k$  as the average skew ratio between  $c_0$  and  $c_k$  over all sink pairs.

We further define the maximum skew variation across corners, for each sink pair  $(f_i, f_{i'})$ , as

$$V_{i,i'} = \max_{\forall (c_k, c_{k'})} v_{i,i'}^{c_k,c_{k'}} \quad (2)$$

Based on the above, we address the following problem formulation: **Skew Variation Reduction Problem.** Given a routed clock tree, minimize the sum over all sink pairs of the maximum normalized skew variation across all corners.

$$\text{Minimize } \sum_{\forall (f_i, f_{i'})} V_{i,i'} \quad (3)$$

<sup>1</sup>A crosslink is an additional wire between any two nodes of a given clock tree.

## 4. OPTIMIZATION FRAMEWORK

Figure 1 illustrates our optimization framework. We perform global and local optimizations to reduce skew variations. The global optimization constructs a linear program (LP) and uses it to guide buffer insertion, buffer removal, and routing detours. Local optimization is based on a machine learning-based predictor of latency changes. It iteratively minimizes skew variation via tree surgery (i.e., driver reassignment), buffer sizing, and buffer displacement. The iterative optimization continues until there is no further improvement or other stopping condition is reached.

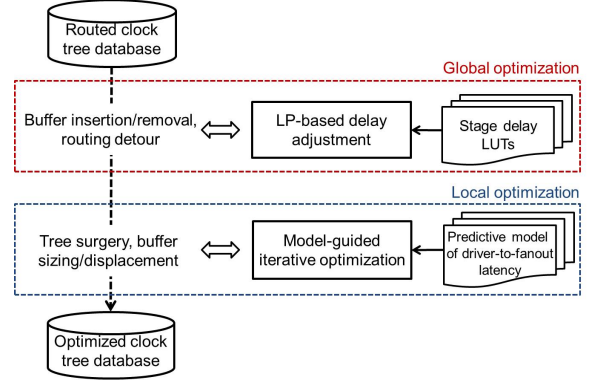


**Figure 1: Overview of our optimization framework.**

### 4.1 Global Optimization

We construct a linear program (LP) to reduce the sum of skew variations between all sink pairs in a clock tree. Based on the LP solution, we determine the desired delay changes of arcs at all corners and perform buffer insertion and removal, as well as routing detour, to accomplish the desired delay changes. We determine number of buffers, buffer size and length of routing detour based on lookup tables. However, the achievable delay values are discrete due to the limited number of buffer sizes. Further, placement legalization and routing congestion also lead to discrepancy between desired delay and actual delay after ECOs in the P&R tool. Therefore, to minimize the sum of skew variations as well as to increase the likelihood that the solution is practically implementable, we formulate the LP such that it minimizes the total amount of delay changes with respect to an upper bound on sum of skew variations. As a result, we implicitly minimize the number of ECO changes. We then sweep this upper bound to search for the achievable solution with minimum sum of skew variations. The objective function is:

$$\text{Minimize } \sum_{1 \leq j \leq M, 0 \leq k \leq K} |\Delta_j^k| \quad (4)$$

where  $\Delta_j^k$  is the latency change on arc  $s_j$  at corner  $c_k$ .<sup>2</sup> The upper bound  $U$  on the sum of skew variations is specified as

$$\sum_{(f_i, f_{i'})} V_{i,i'} \leq U \quad (5)$$

where  $V_{i,i'}$  is the maximum normalized skew variation for the sink pair  $(f_i, f_{i'})$  over all corner pairs  $(c_k, c_{k'})$ , and is calculated based on the following constraint.

$$\begin{aligned} V_{i,i'} &\geq \alpha_k \cdot \left( \sum_{s_j \in P_{i'}} (D_j^{c_k} + \Delta_j^{c_k}) - \sum_{s_j \in P_i} (D_j^{c_k} + \Delta_j^{c_k}) \right) \\ &\quad - \alpha_{k'} \cdot \left( \sum_{s_j \in P_{i'}} (D_j^{c_{k'}} + \Delta_j^{c_{k'}}) - \sum_{s_j \in P_i} (D_j^{c_{k'}} + \Delta_j^{c_{k'}}) \right) \\ V_{i,i'} &\geq \alpha_{k'} \cdot \left( \sum_{s_j \in P_{i'}} (D_j^{c_{k'}} + \Delta_j^{c_{k'}}) - \sum_{s_j \in P_i} (D_j^{c_{k'}} + \Delta_j^{c_{k'}}) \right) \\ &\quad - \alpha_k \cdot \left( \sum_{s_j \in P_{i'}} (D_j^{c_k} + \Delta_j^{c_k}) - \sum_{s_j \in P_i} (D_j^{c_k} + \Delta_j^{c_k}) \right) \end{aligned} \quad (6)$$

We further constrain the optimization such that the solution returned does not degrade (i) local skew at any corner, nor (ii) the

<sup>2</sup>We formulate  $\Delta_j^k$  as positive and negative components to handle the absolute values in our formulation.

skew variation between corner pairs  $(c_k, c_0)$ , for all arcs on clock paths at all non-nominal corners  $c_k$ .

$$\sum_{s_j \in P_f} (D_{j'}^{c_k} + \Delta_{j'}^{c_k}) - \sum_{s_j \in P_i} (D_j^{c_k} + \Delta_j^{c_k}) \leq \left| \sum_{s_j \in P_f} D_{j'}^{c_k} - \sum_{s_j \in P_i} D_j^{c_k} \right|$$

$$\sum_{s_j \in P_i} (D_j^{c_k} + \Delta_j^{c_k}) - \sum_{s_j \in P_f} (D_{j'}^{c_k} + \Delta_{j'}^{c_k}) \leq \left| \sum_{s_j \in P_f} D_{j'}^{c_k} - \sum_{s_j \in P_i} D_j^{c_k} \right| \quad (7)$$

$$\alpha_k \cdot \left( \sum_{s_j \in P_f} (D_{j'}^{c_k} + \Delta_{j'}^{c_k}) - \sum_{s_j \in P_i} (D_j^{c_k} + \Delta_j^{c_k}) \right) - \sum_{s_j \in P_f} (D_{j'}^{c_0} + \Delta_{j'}^{c_0}) - \sum_{s_j \in P_i} (D_j^{c_0} + \Delta_j^{c_0})$$

$$\leq \left| \alpha_k \cdot \left( \sum_{s_j \in P_f} D_{j'}^{c_k} - \sum_{s_j \in P_i} D_j^{c_k} \right) - \left( \sum_{s_j \in P_f} D_{j'}^{c_0} - \sum_{s_j \in P_i} D_j^{c_0} \right) \right|$$

$$\sum_{s_j \in P_f} (D_{j'}^{c_0} + \Delta_{j'}^{c_0}) - \sum_{s_j \in P_i} (D_j^{c_0} + \Delta_j^{c_0}) - \alpha_k \cdot \left( \sum_{s_j \in P_f} (D_{j'}^{c_k} + \Delta_{j'}^{c_k}) - \sum_{s_j \in P_i} (D_j^{c_k} + \Delta_j^{c_k}) \right)$$

$$\leq \left| \alpha_k \cdot \left( \sum_{s_j \in P_f} D_{j'}^{c_k} - \sum_{s_j \in P_i} D_j^{c_k} \right) - \left( \sum_{s_j \in P_f} D_{j'}^{c_0} - \sum_{s_j \in P_i} D_j^{c_0} \right) \right| \quad (8)$$

We also bound the maximum latency for each clock path as follows.

$$\sum_{s_j \in P_i} (D_j^{c_k} + \Delta_j^{c_k}) \leq D_{max} \quad (9)$$

For each arc, we specify the upper and lower bounds on the latency change. The lower bound  $D_{min,j}^{c_k}$  is determined by the delay with optimal buffer insertion, without any routing detour. The upper bound of delay change is defined as  $\beta$  times of the original arc delay, in which  $\beta$  can be selected empirically (we assume  $\beta = 1.2$  in this work).

$$D_{min,j}^{c_k} \leq D_j^{c_k} + \Delta_j^{c_k} \leq \beta \cdot D_j^{c_k} \quad (10)$$

To increase the likelihood that the LP solution is practically implementable, we characterize lookup tables at each corner for stage delays of inverter pairs<sup>3</sup> with various gate sizes and routed wirelengths between consecutive inverters. We define the stage delay between inverter pairs as the sum of gate delays of the two inverters in a pair and the delays of their fanout nets (Figure 3). Based on the characterized lookup tables, we observe that for a given stage delay per unit distance at  $c_0$  (i.e., the ratio between stage delay and routed wirelength for an inverter pair), the stage delay ratios between pairs of corners  $(c_0, c_1)$  and  $(c_0, c_2)$ , respectively. In the plot, each circle represents an inverter pair with a particular gate size, routed wirelength between consecutive inverters, input slew and load capacitance. We use polynomial fit to determine upper ( $W_{max}^{c_k, c_l}$ ) and lower ( $W_{min}^{c_k, c_l}$ ) bounds of delay ratios for each pair of corners, which are shown as the red curves. Any delay ratio larger (smaller) than the upper (lower) bound is not achievable with available buffer insertion solutions in lookup tables. Furthermore, we assume that the delay per unit distance of an arc does not vary significantly in our optimization due to Constraints (7)-(10). Thus, we use delay per unit distance of an arc in the original clock tree to estimate upper and lower bounds of delay ratios ( $W_{min,max}^{c_k, c_l}$ ), and apply these bounds in Constraint (11) to avoid LP solutions that are not practically implementable by ECOs.

$$W_{min}^{c_k, c_l} \leq \frac{D_j^{c_k} + \Delta_j^{c_k}}{D_{j'}^{c_l} + \Delta_{j'}^{c_l}} \leq W_{max}^{c_k, c_l} \quad (11)$$

**Complexity Analysis.** The LP formulation (Equations (4)-(11)) has  $O(M \cdot K)$  variables to indicate delay change on each arc at each corner ( $\Delta_j^{c_k}$ ); there are also  $O(N^2)$  (i.e., the number of

<sup>3</sup>In this work, we assume that the buffers used to construct the clock tree are comprised of inverter pairs. But, our methodologies apply to clock trees with both inverting and non-inverting buffers.

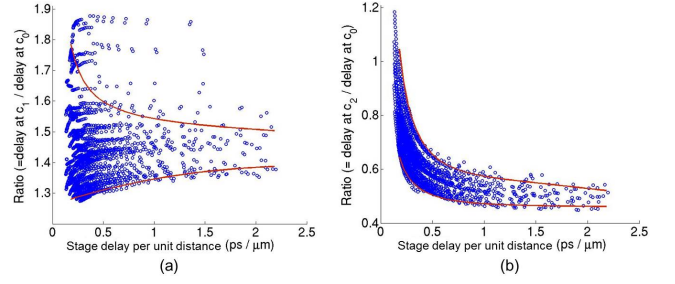


**Figure 2: Delay ratios between  $(c_1, c_0)$  and  $(c_2, c_0)$ , respectively.  $c_0 = (\text{SS}, 0.9\text{V}, -25^\circ\text{C}, \text{Cmax})$ ,  $c_1 = (\text{SS}, 0.75\text{V}, -25^\circ\text{C}, \text{Cmax})$  and  $c_2 = (\text{FF}, 1.1\text{V}, 125^\circ\text{C}, \text{Cmin})$ .**

sink pairs) variables to indicate the maximum normalized skew variation across all corner pairs between each sink pair ( $V_{i,i'}$ ). There are  $C(K,2)$  constraints to force  $V_{i,i'}$  to be no less than the maximum normalized skew variation between each sink pair (Constraint (6));  $(4 \cdot K)$  constraints to prevent local skew and skew variation degradations (Constraints (7)-(8));  $N$  constraints to specify the maximum latency (Constraint (9));  $(2 \cdot M)$  constraints to bound arc delay changes (Constraint (10)); and  $C(K,2)$  constraints to enhance ECO feasibility (Constraint (11)).

**ECO Implementation.** We apply ECO changes to accomplish the desired arc delays at each corner, which are determined by LP solution. Given that the buffer insertion problem is NP-complete [19], although we apply several techniques to enhance ECO feasibility, the LP formulation still cannot guarantee an optimal solution that is practically implementable. Thus, our target is to minimize the discrepancy between the desired delays in the LP solution and those that actually result from ECOs. In our ECO implementation, we first remove all original inverter pairs on the arc. We then determine the solution (i.e., gate size and routed wirelengths between consecutive inverters) of inverter pair insertion based on the characterized lookup tables with stage delays. Note that in this work, we always use one gate size, and uniformly place inverter pairs, for each individual arc. We place inverter pairs in a “U” shape when routing detour is required. The lookup table contains stage delays with five inverter sizes and routed wirelengths between consecutive inverters varying from  $10\mu\text{m}$  to  $200\mu\text{m}$  with a step size of  $5\mu\text{m}$  across different corners. Since these lookup tables are technology-dependent, we only perform the characterization once per technology. More specifically, we have two lookup tables: (i)  $LUT_{detail}$  is characterized with different input slew and fanout load capacitance, and is applied for the first and last inverter pairs of a given arc, and (ii)  $LUT_{uniform}$  is characterized based on average stage delay of inverter pairs in an arc, and is applied for the inverter pairs in the middle of an arc (Figure 3).

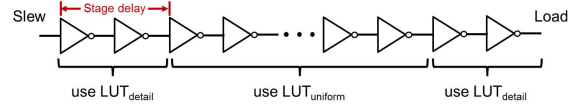


**Figure 3:  $LUT_{detail}$  is characterized with various input slews and fanout loads capacitance;  $LUT_{uniform}$  contains average stage delay with particular gate size and routed wirelengths between consecutive inverters.**

Algorithm 1 describes the flow to select solutions for inverter pair insertions. For each combination of gate size and routed wirelength between consecutive inverters, we estimate a range of desired number of inverter pairs (i.e.,  $[\max(u_{est} - 2, 0), u_{est} + 2]$ ) based on the average stage delay in  $LUT_{uniform}$  at corner  $c_0$  (Lines 5-6).  $D_{LP}^{c_k}$  is the required arc delay at corner  $c_k$  in the LP solution. We then assess error for each potential solution (i.e., a combination of gate size, routed wirelength between consecutive inverters and number of inverter pairs) and select the solution with minimum error (Lines 7-16). We use  $p$  and  $q$  to respectively index the gate size and the routed wirelength between consecutive inverters.  $D_{est}^{c_k}$  is the estimated delay using LUTs. Last, we implement ECO changes based on the selected solution (Lines 19, 21).

**Algorithm 1** LP-guided ECO flow.

```

1: for all  $s_j$  to be optimized do
2:   Remove current inverter pairs on  $s_j$ 
3:    $err_{min} \leftarrow +\infty$ ;  $sol \leftarrow \emptyset$ 
4:   for  $p := 1$  to  $N_{size}$ ,  $q := 1$  to  $N_{WL}$  do
5:      $u_{est} \leftarrow \text{round}(D_{LP}^k / d(LUT_{uniform})_{p,q}^{c_k})$ 
6:     for  $u := \max(u_{est} - 2, 0)$  to  $u_{est} + 2$  do
7:        $err \leftarrow 0$ 
8:       for  $k := 0$  to  $K$  do
9:          $err \leftarrow err + |D_{est}^k - D_{LP}^k|$ 
10:      end for
11:      for all corner pair  $(c_k, c_{k'})$  do
12:         $err \leftarrow err + |(D_{est}^k - D_{est}^{k'}) - (D_{LP}^k - D_{LP}^{k'})|$ 
13:      end for
14:      if  $err < err_{min}$  then
15:         $err_{min} \leftarrow err$ ;  $sol \leftarrow (p, q, u)$ 
16:      end if
17:    end for
18:  end for
19:  Perform ECO inverter pair insertion based on  $sol$ 
20: end for
21: Legalize all inserted inverters and perform ECO routing

```

## 4.2 Local Optimization

We apply local iterative optimization to further minimize the sum of skew variations across corners. More specifically, we consider three types of local moves, which are illustrated in Figure 4(b)-(d) – (I) buffer sizing and/or buffer displacement, (II) displacement of a buffer and gate sizing on one of its child buffers, and (III) tree surgery (i.e., reassignment of a (child) node to a different (parent) driver). However, performance of such iterative optimization is usually limited by its large turnaround time. For instance, each local move requires placement legalization, ECO routing, parasitic extraction, and timing analysis in the golden timer.<sup>4</sup> Given such large turnaround time, it is practically impossible to explore all possible local moves for a given design. Therefore, a fast and accurate model to predict the impact of local moves is necessary. Previous work [8] has demonstrated that machine learning-based models are quite accurate for delay and slew estimation. In our work, we apply a two-stage machine learning-based model for prediction of arc delay changes with local moves. The overarching goal is to be able to accurately predict *delta-latency*, i.e., the change in post-ECO routing source-sink delays that results from a given buffer’s resizing and/or placement perturbation.

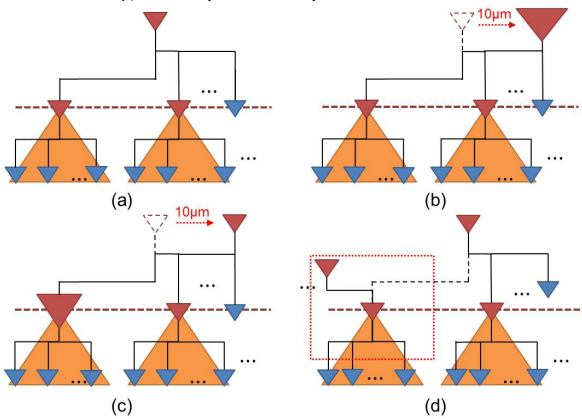


**Figure 4: Local optimization moves used in our flow. (a) Initial subtree; (b) sizing and/or displacement, (c) displacement and sizing of child node, and (d) tree surgery, i.e., driver reassignment.**

**Machine Learning-Based Model.** To predict the impact of a local move, we first estimate new routing pattern (if the move contains displacement or tree surgery) by constructing two types of trees – FLUTE [3] tree and single-trunk Steiner tree. We approximate wire delays correspondingly using Elmore delay and D2M [1] models.

<sup>4</sup>In our experiments, the runtime for each local move on a testcase with 1.79M instances and 270K flip-flops, using one thread per analysis corner on a 2.5GHz Intel Xeon server, is around 70 minutes (i.e., 30 minutes for ECO and parasitic extraction, and 40 minutes for timing analysis).

We then update the delay and output slew of the driver based on the estimated wire capacitance and update pin capacitance (if the move sizes the child node) by performing interpolation in the Liberty table. Last, we perform slew propagation using PERI [14] and update gate delays one and two stages downstream based on Liberty tables.<sup>5</sup> However, as observed in [8], the interpolated delay values do not always match those from the golden timer’s analysis. Further, the estimated routing pattern as well as wire delay can have discrepancy with respect to the commercial router’s actual ECO solution.

We therefore construct machine learning-based models to minimize such discrepancy. We use Artificial Neural Networks (ANN) [9], Support Vector Machines (SVM) with a Radial Basis Function (RBF) kernel [9], and Hybrid Surrogate Modeling (HSM) [13].<sup>6</sup> In addition to the estimated delays based on {FLUTE tree, single-trunk Steiner tree}  $\times$  {Elmore delay, D2M}, the input parameters to the machine learning-based model also include the number of fanout cells, as well as the area and aspect ratio of the bounding box which contains driving pin and fanout cells. To generate training data, we construct artificial testcases (i.e., clock trees) that resemble real designs with fanout ranging from 1-5 (20-40 for last-stage buffers) and bounding box area and aspect ratio of the driven pins ranging from  $1000\mu\text{m}^2$  to  $8000\mu\text{m}^2$  and from 0.5 to 1, respectively. We then place fanout cells or sinks randomly within the bounding box. We generate 150 artificial testcases and perform 450 moves on average to each testcase (the runtime for one testcase is  $\sim 1$  hour). Note that we only construct one model for each corner, and that this model is applied to all designs.

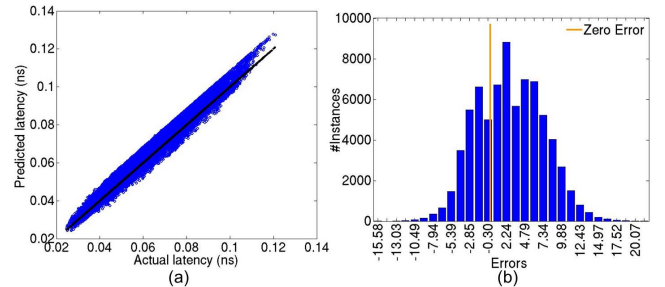


**Figure 5: Examples of (a) predicted vs. actual latencies, and (b) percentage error histograms from our model for  $c_3$  corner in Table 3.**

We create one delta-latency model for each corner used in our experiments. Figure 5(a) shows the predicted vs. actual latencies that we compute from the predicted delta latencies by our model at corner  $c_3$  in Table 3. Figure 5(b) shows the corresponding histogram of percentage errors. Across all the corners, our modeling error is 2.8% on average. The absolute of maximum and minimum errors are 21.98% and 16.21% respectively. The modeling for each corner using the artificial testcases is a one-time effort. On a 2.5GHz Intel Xeon server, the time to train a model for each corner is around 5 hours with four threads. Models for each corner can be trained in parallel, e.g., on a server with 24 threads, we can train six models in 5 hours. Our models generalize to different testcases because (i) our training dataset generated from the artificial testcases span ranges of parameters that are typically seen in clock trees in SOC application processors and memory controllers, and (ii) we prevent overfitting by performing cross-validation. Our experimental results indicate that our models are generalizable and accurate when applied to “unseen” testcases during the model training phase. Figure 6 shows the accuracy comparison between our learning-based model and analytical models. We observe that with fewer attempts, our learning-based model is able to identify the best move for more buffers.

**Iterative Optimization Flow.** Based on our model, we perform iterative local optimization flow illustrated in Algorithm 2. We first enumerate all candidate local moves and generate the input data to our model (Line 1). The moves we consider in this work are

<sup>5</sup>Our analyses show that the delay and slew change of buffers beyond two stages is  $< 1ps$ , so we do not update timings of buffers beyond two stages downstream.

<sup>6</sup>Further details of the applied machine-learning techniques that we use may be found in [9] and [13].

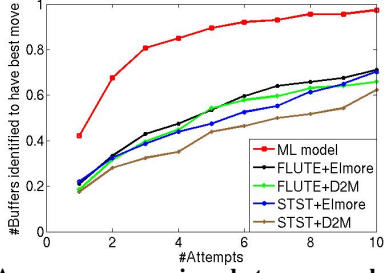


**Figure 6: Accuracy comparison between our learning-based model and analytical models. An attempt is an ECO. There are 114 buffers, and each buffer has 45 candidate moves. In one attempt, the learning-based model (resp. analytical models) can identify best moves for 40% (resp. up to 20%) of the buffers.**

shown in Table 2. We predict the delta-latency resulting from each move based on our model (Line 2). We then estimate the skew variation reductions based on the predicted latency changes. Our experimental results show that we are able to evaluate the impacts of more than 160K moves at three corners in 17 min on a 2.5GHz Intel Xeon server with 15 threads. We sort the candidate moves in decreasing order of their predicted skew variation reductions, and pick the top  $R$  (i.e.,  $R = 5$  in this work) moves to implement in  $R$  individual threads (Line 3). Last, we perform timing analysis using the golden timer to assess the actual skew variation changes (Line 4). If there is skew variation reduction, we update the database with the minimum skew variation solution. Otherwise, we implement the next  $R$  moves (Lines 5-9). The iteration terminates when there is no move showing skew variation reduction according to our predictor.

#### Algorithm 2 Iterative optimization flow.

- 1: Enumerate all candidate moves and generate input data to model
- 2: Predict delta-latency and skew variation reductions
- 3: Implement  $R$  moves with maximum predicted skew variation reductions using  $R$  threads
- 4: Assess actual skew variation reductions with the golden timer
- 5: **if** there is skew variation reduction **then**
- 6:   Update database with the minimum skew variation solution
- 7: **else**
- 8:   Implement the next  $R$  moves and go to Line 4
- 9: **end if**

**Table 2: Candidate moves in our optimization.**

Type	Candidate moves
I	displace {N, S, E, W, NE, NW, SE, SW} by $10\mu\text{m} \times$ one-step up/down sizing
II	displace {N, S, E, W, NE, NW, SE, SW} by $10\mu\text{m} \times$ one-step up/down sizing on one child node
III	reassign to a new driver (i) at the same level as current driver, and (ii) within bounding box of $50\mu\text{m} \times 50\mu\text{m}$

## 5. EXPERIMENTAL RESULTS

Our experiments are implemented in foundry 28nm LP technology. We construct the original clock tree and perform ECO optimizations using *Synopsys IC Compiler* [25]. We use *Synopsys PrimeTime* [26] and *Synopsys PT-PX* for timing and power analyses, respectively. We construct the machine learning-based model using *MATLAB* [24]. The optimization flow is implemented using C++ and Tcl scripts.

### 5.1 Testcase Description

We have developed two classes of testcase generators to validate our proposed optimization framework. Class **CLS1** corresponds to clock networks typically observed in high-speed application processors and graphics processors. Class **CLS2** corresponds to clock networks in memory controllers, which are typically used in SoCs to interface SoC components with DRAM/eDRAM. We implement our testcases at 28nm LP technology. The corners used in our experiments are shown in Table 3. We use the testcase generation methodology described in [5], and the top-level structures of the testcases T1 and T2 in [5]. We modify the floorplan and clock tree synthesis flow to develop two variants of CLS1, **CLS1v1** and **CLS1v2**. Each of **CLS1v1** and **CLS1v2** contains four identical  $650\mu\text{m} \times 650\mu\text{m}$  interface logic modules

(ILMs) to resemble four cores of an application processor. These are floorplanned in a rectangular block such that the utilization of standard cells is  $\sim 60\%$  before placement.<sup>7</sup> Figure 7(a) shows the floorplan of **CLS1v1**. We implement the CLS1 class testcases at corners  $c_0$ ,  $c_1$  and  $c_3$  as shown in Table 4. Corners  $c_0$  and  $c_1$  are setup-critical, and  $c_3$  is hold-critical. Table 4 summarizes various post-synthesis metrics of these testcases.

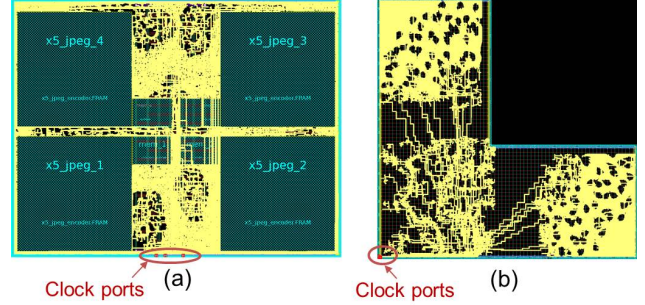


**Figure 7: Floorplans of (a) CLS1v1, and (b) CLS2v1. In yellow are routed clock nets.**

**Table 3: Description of corners.**

Corner	Process	Voltage	Temperature	Back-end-of-line
$c_0$	ss	0.90V	-25°C	Cmax
$c_1$	ss	0.75V	-25°C	Cmax
$c_2$	ff	1.10V	125°C	Cmin
$c_3$	ff	1.32V	125°C	Cmin

**Table 4: Summary of testcases.**

Testcase	#Cells	#Flip-flops	Area	Util	Corners
<b>CLS1v1</b>	0.4M	36K	$3.3\text{mm}^2$	62%	$c_0, c_1, c_3$
<b>CLS1v2</b>	0.4M	35K	$3.4\text{mm}^2$	60%	$c_0, c_1, c_3$
<b>CLS2v1</b>	1.79M	270K	$4.5\text{mm}^2$	58%	$c_0, c_1, c_2$

We also study a testcase **CLS2v1** of class memory controller, which is new as compared to [5]. Table 4 summarizes the post-synthesis metrics of this testcase, and Figure 7(b) shows its floorplan. We use the methodology described in [5] to generate random logic and connect this logic to FFs; this includes datapaths across different clock groups. The memory controller is floorplanned in an L-shaped block with the controller at the center and the interface logic in each of the top and bottom arms of the L-shape. The interface logic has data and control signals across memory, processor and other blocks. The control signals are generated within the controller, and the FFs in the interface logic and controller are separated by large distances (e.g.,  $\sim 1\text{mm}$ ). The large distance between sequentially adjacent sinks leads to large clock skew, which the commercial tool tries to balance by inserting buffers. However, these clock buffers lead to skew variations across corners. We implement the **CLS2v1** testcase at corners  $c_0$ ,  $c_1$  and  $c_2$  as shown in Table 4, where  $c_0$  and  $c_1$  are setup-critical and  $c_2$  is hold-critical.

For implementations of all our testcases, we follow a production methodology [23]. We set the skew target as  $0\text{ps}$  in the CTS tools, as our studies (with skew targets ranging from  $0\text{ps}$  to  $250\text{ps}$ , in steps of  $50\text{ps}$ ) indicate that a target skew of  $0\text{ps}$  steers the tool to deliver the smallest skew at each corner. We perform clock tree optimizations with both multi-corner multi-mode (MCM) scenario as well as multi-corner single-mode (MCSM) scenario at each mode. We then select the optimized clock tree solution with minimum skew variation as the input to our optimization.

### 5.2 Results

Table 5 shows the experimental results,<sup>8</sup> where **variation**, **skew**, **#cells**, **power** and **area** are respectively the sum of normalized skew variations over union of top 10K critical sink pairs (in terms of setup and hold timing slacks) at each corner,<sup>9</sup> local skew at each corner, total number of clock cells, clock tree power and total area of clock cells. In the experiments, we apply three

<sup>7</sup>We understand from our industry collaborators that best-practices flows for high-speed and memory controller blocks start with 50%–60% utilization before placement [23].

<sup>8</sup>Our optimization does not create any maximum transition or maximum capacitance violations.

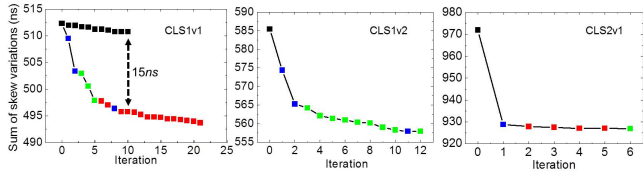
<sup>9</sup>The number of optimized sink pairs for **CLS1v1**, **CLS1v2** and **CLS2v2** are respectively 15012, 14671 and 15142.

optimization flows to each of the testcases: (i) *global* is the global optimization flow, (ii) *local* is the local iterative optimization flow, and (iii) *global-local* performs global and local optimizations in sequence. The global (local) optimization alone achieves up to 16% (5%) reduction on the sum of skew variations. Since local moves affect only a subset of sink pairs, they have smaller impact than that of the global optimization. By combining the two optimizations, we reduce the sum of skew variations by 22% with negligible area and power overhead. The results also show no degradation of local skews. Further, we observe that the local iterative optimization reduces skew variations more when applied after the global optimization, as compared to a standalone local skew optimization (e.g., for **CLS1v1**, local optimization achieves 13ns more reduction with a prior global optimization, as compared to the standalone local optimization).

**Table 5: Experimental results.**

Testcase	Flow	Variation [norm] (ns)	Skew (ps)			#Cells	Power (mW)	Area ( $\mu\text{m}^2$ )
			$c_0$	$c_1$	$c_{2,3}$			
<b>CLS1v1</b>	<i>orig</i>	512 [1.00]	214	530	226	2515	0.355	3615
	<i>global</i>	431 [0.84]	179	395	188	2553	0.356	3705
	<i>local</i>	493 [0.96]	214	529	223	2515	0.355	3621
	<i>global-local</i>	399 [0.78]	175	387	188	2553	0.356	3706
<b>CLS1v2</b>	<i>orig</i>	585 [1.00]	272	594	259	2762	0.369	3968
	<i>global</i>	518 [0.89]	269	575	235	2762	0.369	3975
	<i>local</i>	557 [0.95]	258	545	259	2762	0.369	3970
	<i>global-local</i>	510 [0.87]	265	564	235	2762	0.369	3975
<b>CLS2v1</b>	<i>orig</i>	972 [1.00]	179	192	282	5568	0.865	8556
	<i>global</i>	888 [0.91]	175	192	232	5574	0.866	8577
	<i>local</i>	926 [0.95]	180	190	282	5568	0.865	8556
	<i>global-local</i>	841 [0.87]	176	192	232	5574	0.866	8557

Figure 8 shows the skew variation reduction during the local iterative optimization. We observe that tree surgeries (type-I moves) are more effective than sizing and displacement moves (type-II and type-III moves), and are applied by our model in the early iterations. For **CLS1v1**, we also show the results with 10 random moves (dots in black), where the gap between random move and our optimization is 15ns. This validates the benefits of our delta-latency model. The runtimes per iteration (with 15 threads) are 60 min, 80 min and 200 min for testcases **CLS1v1**, **CLS1v2** and **CLS2v1**, respectively.



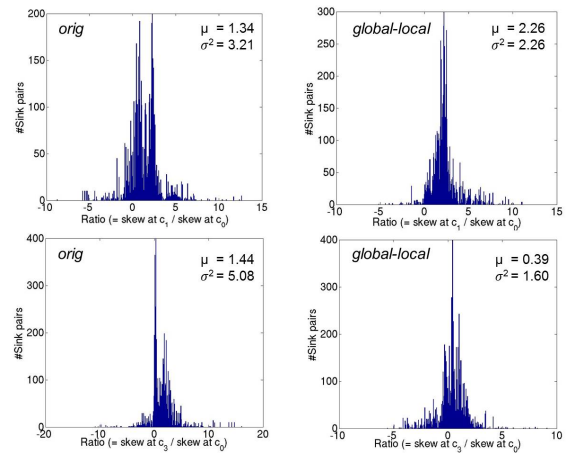
**Figure 8: Sum of skew variations reduces during the local iterative optimization. In blue are type-I moves, in red are type-II moves, and in green are type-III moves.**

Figure 9 shows the distributions of skew ratios between corner pairs ( $c_1, c_0$ ) and ( $c_3, c_0$ ), over sink pairs, of the initial clock tree and the optimized clock tree. We observe that our optimization significantly reduces the variation and range of skew ratios between corner pairs.

## 6. CONCLUSION

In this work, we propose the first framework to minimize the sum of skew variations over all sequentially adjacent sink pairs, using both global and local optimizations. Our experimental results show that the proposed flow achieves up to 22% reduction of the sum of skew variations for testcases implemented in foundry 28nm technology, as compared to a leading commercial tool. In the global optimization, our LP formulation comprehends the ECO feasibility based on characterized lookup tables of stage delays. In the local optimization, we demonstrate that machine learning-based predictors of latency changes can provide accurate estimation of local move impacts.

Our future works include: (i) study of the resultant power and area benefits of reduced skew variation; (ii) development of models to predict a buffer location for minimum skew over a continuous range of possible buffer locations; (iii) explorations, motivated by our current results, of new library cells whose delay and slew are



**Figure 9: Distribution of skew ratios between ( $c_1, c_0$ ) and ( $c_3, c_0$ ) of (i) original clock tree, and (ii) optimized clock tree for **CLS1v1**.**

less sensitive to corner variation so as to enable fine-grained ECOs based on our LP solutions; and (iv) investigation of whether a worse initial start point (clock network with large skew variations) can enable us to achieve smaller skew variation across corners using our optimization flow.

## 7. REFERENCES

- [1] C. J. Alpert, A. Devgan and C. Kashyap, “A Two Moment RC Delay Metric for Performance Optimization”, *Proc. ISPD*, 2000, pp. 73-78.
- [2] J. Bhasker and R. Chadha, *Static Timing Analysis for Nanometer Designs: A Practical Approach*, Springer, 2009.
- [3] C. Chu, “FLUTE: Fast Lookup Table Based Wirelength Estimation Technique”, *Proc. ICCAD*, 2004, pp. 73-76.
- [4] A. Cao, S.-M. Chang and D.-C. Yuan, “Local Clock Skew Optimization”, *US Patent No. 8,635,579*, 2014.
- [5] T.-B. Chan, K. Han, A. B. Kahng, J.-G. Lee and S. Nath, “OCV-Aware Top-Level Clock Tree Optimization”, *Proc. GLSVLSI*, 2014, pp. 33-38.
- [6] M. Cho, S. Ahmed and D. Z. Pan, “TACO: Temperature Aware Clock-tree Optimization”, *Proc. ICCAD*, 2005, pp. 582-587.
- [7] H.-M. Chou, H. Yu and S.-C. Chang, “Useful-Skew Clock Optimization for Multi-Power Mode Designs”, *Proc. ICCAD*, 2011, pp. 647-650.
- [8] S. S. Han, A. B. Kahng, S. Nath and A. Vydyanathan, “A Deep Learning Methodology to Proliferate Golden Signoff Timing”, *Proc. DATE*, 2014, pp. 1-6.
- [9] T. Hastie, R. Tibshirani and J. Friedman, *The Elements of Statistical Learning: Data Mining, Inference, and Prediction*, Springer, 2009.
- [10] C.-L. Lung, H.-C. Hsiao, Z.-Y. Zeng and S.-Y. Chang, “LP-Based Multi-Mode Multi-Corner Clock Skew Optimization”, *Proc. VLSI-DAT*, 2010, pp. 335-338.
- [11] C.-L. Lung, Z.-Y. Zeng, C.-H. Chou and S.-Y. Chang, “Clock Skew Optimization Considering Complicated Power Modes”, *Proc. DATE*, 2010, pp. 1474-1479.
- [12] A. B. Kahng, J. Lienig, I. L. Markov and J. Hu, *VLSI Physical Design: From Graph Partitioning to Timing Closure*, Springer, 2011.
- [13] A. B. Kahng, B. Lin and S. Nath, “Enhanced Metamodeling Techniques for High-Dimensional IC Design Estimation Problems”, *Proc. DATE*, 2013, pp. 1861-1866.
- [14] C. V. Kashyap, C. J. Alpert, F. Liu and A. Devgan, “PERI: A Technique for Extending Delay and Slew Metrics to Ramp Inputs”, *Proc. TAU*, 2002, pp. 57-62.
- [15] T. Mittal and C.-K. Koh, “Cross Link Insertion for Improving Tolerance to Variations in Clock Network Synthesis”, *Proc. ISPD*, 2011, pp. 29-36.
- [16] A. Rajaram, J. Hu and R. Mahapatra, “Reducing Clock Skew Variability via Crosslinks”, *Proc. DAC*, 2004, pp. 18-23.
- [17] A. Rajaram and D. Z. Pan, “Variation Tolerant Buffered Clock Network Synthesis with Cross Links”, *Proc. ISPD*, 2006, pp. 157-164.
- [18] P. J. Restle, T. G. McNamara, D. A. Webber, P. J. Camporese, K. F. Eng, K. A. Jenkins, D. H. Allen, M. J. Rohn, M. P. Quaranta, D. W. Boerstler, C. J. Alpert, C. A. Carter, R. N. Bailey, J. G. Petrovick, B. L. Krauter, and B. D. McCredie, “A Clock Distribution Network for Microprocessors”, *IEEE J. Solid-State Circuits* 36(5) (2001), pp. 792-799.
- [19] W. Shi and Z. Li and C. Alpert, “Complexity Analysis and Speedup Techniques for Optimal Buffer Insertion with Minimum Cost”, *Proc. ASPDAC*, 2004, pp. 609-614.
- [20] H. Su and S. S. Sapatnekar, “Hybrid Structured Clock Network Construction”, *Proc. ICCAD*, 2001, pp. 333-336.
- [21] S. Sunder and K. Scholtman, “Multi-Mode Multi-Corner Clocktree Synthesis”, *US Patent No. US2009021725 A1*, 2009.
- [22] G. Venkataraman, N. Jayakumar, J. Hu, P. Li and S. Khatri, “Practical Techniques to Reduce Skew and Its Variations in Buffered Clock Networks”, *Proc. ICCAD*, 2005, pp. 592-596.
- [23] Samsung Electronics Corporation (System LSI application processor principal engineer), *personal communication*, July 2014.
- [24] “MATLAB.” <http://www.mathworks.com/products/matlab/>
- [25] “Synopsys IC Compiler User Guide.”
- [26] “Synopsys PrimeTime User’s Manual.”